

Enhancing Haptic Detection of Surface Undulation

RYO KIKUUWE, AKIHITO SANO, HIROMI MOCHIYAMA, NAOYUKI TAKESUE
Touch Technology Laboratory Funded by Toyota, Nagoya Institute of Technology
and
HIDEO FUJIMOTO
Robotics and Automation Laboratory, Nagoya Institute of Technology

This paper introduces a device for enhancing detection of surface undulation through active touch. This device, which we call a “tactile contact lens,” is composed of a sheet and numerous pins arranged on one side of the sheet. Experimental results show that a small bump on a surface can be detected more accurately through this device than by bare finger and than through a flat sheet. A mathematical analysis of this phenomenon suggests two possible explanations for this phenomenon. One lies in the lever-like behavior of the pins. The pins convert the local inclination of the object surface into the tangential displacement of the skin surface. The second is the spatial aliasing effect resulting from the discrete contact. Due to this effect, the temporal change in the skin surface displacement is efficiently transduced into the temporal change in the skin tissue strain. The results of this analysis are then discussed in relation to other sensitivity-enhancing materials, tactile sensing mechanisms, and tactile/haptic display devices.

Categories and Subject Descriptors: B.m [**Hardware**]: Miscellaneous; H.1.2 [**Models and Principles**]: User/Machine Systems—*Human factors*; H.5.2 [**Information Interfaces and Presentation**]: User Interfaces—*Haptic I/O*

General Terms: Human factors, Theory, Verification

Additional Key Words and Phrases: Haptics, sensation enhancement, surface undulation, tactile contact lens, tactile sensing

1. INTRODUCTION

In today’s automobile industry, the surfaces of metal sheets are still inspected by craftworkers’ touch. They have long known that they can detect small deflection defects on the surface easier when using knit work gloves than when using bare hands.

Some researchers have investigated the effects of gloves for the purpose of preventing loss of dexterity and tactility while maintaining the strength of the gloves [Nelson and Mital 1995; Shibata and Howe 1999]. A few reports have referred to touch-enhancing phenomena elicited by the use of some intermediate objects. Gordon and Cooper [1975] reported that a thin intermediate paper improved the accuracy of detecting orientation of very slight undulation of a surface when the paper was placed between the surface and the hand and was moved by the hand.

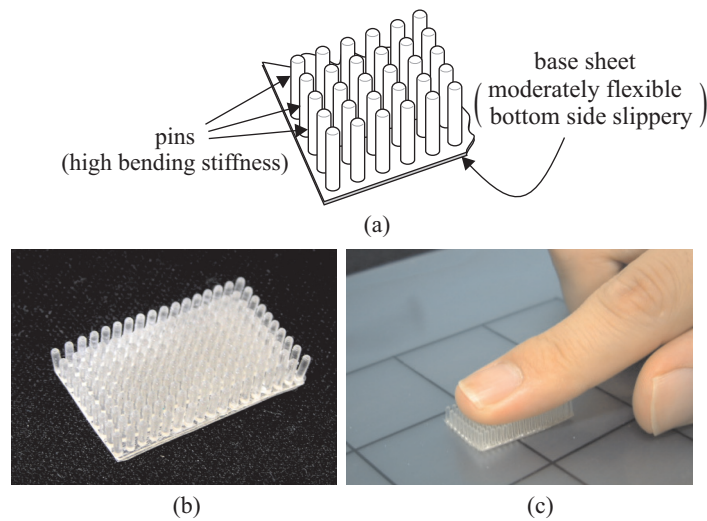


Fig. 1. The tactile contact lens. (a) Basic structure. (b) Photograph of an example prototype. (c) Photograph of the prototype being used on a target surface.

Gordon and Cooper offered the explanation that the intermediate paper reduced the influence of surface roughness, and the sensation of surface undulation was relatively emphasized. This explanation was questioned by Lederman [1978], who reported that the tactile impression of roughness was heightened by the use of a thin intermediate paper. Lederman proposed the explanation that the perception of surface roughness was heightened because the friction force, which usually disturbed tactile perception, was reduced. Lederman also indicated that this explanation might be applied to the enhancement of the perception of surface undulation. The Touch Enhancing Pad [Perry and Wright 1987], which is composed of two thin plastic sheets with a small amount of lubricant enclosed between them, has been approved by the United States Food and Drug Administration (FDA) for use as an aid to breast self-examination to detect stiff lumps. It is generally supposed that the Touch Enhancing Pad's effect is also largely caused by the reduction of friction. To our knowledge, however, this explanation has not been confirmed by scientific studies.

In this paper, we introduce a device for enhancing haptic detection of surface undulation. This device, which we call a “tactile contact lens,” is composed of a sheet and numerous pins regularly arranged on one side of the sheet (Figure 1(a)). This device is supposed to operate not only as a disturbance filter but also as a magnifier of tactile stimuli. Experimental results suggest that a small bump on a surface can be more accurately detected through this device than by bare finger and than through a thin, flat sheet. In addition, a mathematical analysis using the Fourier transform suggests two possible explanations for this phenomenon.

We intend to apply this device to the process of sheet metal inspection in automobile factories, where it will be used to detect small deflection defects on the surface. This inspection has been effected by well-trained craftworkers' touch be-

cause automatic measurement tools, such as laser range sensors, are expensive, inefficient, and easily influenced by extraneous material such as oil spots on the surfaces. The tactile contact lens has no electronic or mechatronic components, and can be manufactured from simple and cost-saving materials. This device is therefore promising for practical applications. Besides, we expect that the touch-enhancing phenomenon induced by this device will provide useful insight into the mechanistic basis of human tactile sensation and into the design of tactile displays and tactile sensors.

The rest of this paper is organized as follows. In section 2, we describe an overview of the tactile contact lens and the results of a psychophysical experiment. Section 3 provides a mathematical analysis, which suggests two causes of the effect of the tactile contact lens. Section 4 discusses the results of the analysis in relation to other sensitivity-enhancing materials, tactile sensing mechanisms, and tactile display devices. This section also discusses future improvements and potential applications of the presented method of analysis. Section 5 provides concluding remarks. The appendix section contains details of the mathematical derivations.

2. THE TACTILE CONTACT LENS

2.1 Overview

The basic structure of the tactile contact lens is illustrated in Figure 1(a). It is composed of a base sheet and numerous pins regularly arranged on one side of the base sheet. When this device is used, the flat side of the base sheet is in contact with a target surface (a surface to be touched), while the other side is pressed by a finger. The device is then moved by the finger across the target surface. The flat side of the base sheet is slippery so that it can be moved smoothly across the target surface. The base sheet is flexible enough to follow the undulation on the target surface easily. At the same time, the base sheet is stiff enough to keep the pins perpendicular to the base sheet even under the pressing force applied by the finger. The pins are as tall as permitted by their bending stiffness and resistance to buckling.

A typical example of the tactile contact lens is shown in Figures 1(b) and (c). The pins and the base sheet are made of photo-curing resin (SL5170, 3D Systems, Inc., Young's modulus of approx. 2400 MPa), and are integrally cast by using a stereolithography device (SLA250, 3D Systems, Inc.). The size of the base sheet is $25 \times 15 \times 0.3$ mm. Each pin is a cylinder with a semispherical end having a diameter 1.0 mm and a length 3.75 mm. The pins are arranged with a pitch of 1.5 mm (i.e., with separations of 0.5 mm) on the base sheet. A piece of tetrafluoroethylene (TFE) film ($25 \times 15 \times 0.09$ mm) is glued to the flat side of the base sheet to facilitate smooth movement on a target surface.

2.2 Experiment

The effectiveness of the tactile contact lens was tested under an experimental condition.

2.2.1 Materials and Methods. Fifteen observers, one woman and 14 men, ranging in age from 21 to 29, participated in the experiment. All observers were students of Nagoya Institute of Technology. All observers classified themselves as

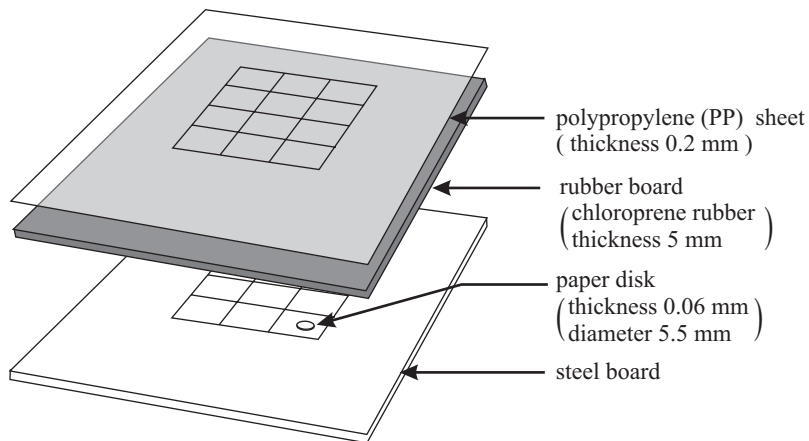


Fig. 2. The experimental apparatus.

right-handed.

We used the experimental apparatus illustrated in Figure 2. It is composed of a steel board, a rubber board (chloroprene rubber, thickness 5 mm), a polypropylene (PP) sheet (thickness 0.2 mm), and a paper disk (a circular piece of paper, thickness 0.06 mm, diameter 5.5 mm). On the steel board, a 4-by-3 grid (each 30 mm square) was drawn. Another 4-by-3 grid was drawn on the PP sheet in the same position and of the same size as that on the steel board. The PP sheet was used in order to mask the surface texture of the rubber board. The paper disk was placed in either of the 12 cells on the steel board. The position of the paper disk appeared as a very gradual bump of a height of approximately 0.06 mm on the surface of the PP sheet. The friction coefficient between the bare finger and the PP sheet ranged approximately from 1.5 to 2.5 (varying by person), whereas that between the TFE film and the PP sheet was approximately 0.25. These values were measured by rubbing a PP sheet glued to a force sensor with a bare-finger and the TFE film.

The observers were asked to detect the cell in which the paper disk existed, and to respond in a forced choice manner. In each trial, the observer was given 6 seconds to rub across the surface of the PP sheet with the index finger of the right hand. Trials were performed in either of three conditions: using the tactile contact lens shown in Figure 1 (the “lens” condition), using an object identical to the tactile contact lens except that it had no pins (the “sheet” condition), and using a bare finger (the “bare-finger” condition). The observers were instructed that the finger should be moved in the finger-to-wrist direction and that the force pressing the surface should be as equal as possible over conditions. Prior to the experiment, the observers performed a few practice trials in every condition after seeing the position of the paper disk.

Each observer performed 12 trials, each of which corresponds to one of the 36 pairs of cell and condition. The 12 pairs presented to each observer were chosen randomly with the following constraints: (1) each observer was presented 12 different cells; (2) each observer was presented four cells under each of three conditions; and (3)

one pair of cell and condition was presented once to every three observers. Order in which the pairs were presented was randomized within each observer.

The observers were not blindfolded, but we can assume that vision did not affect the comparison among the conditions because it was almost impossible to visually detect the bump caused by the paper disk, and because the influence of vision was homogeneous over all three conditions.

2.2.2 Results and Discussions. The total number of trials under each condition was 60 (4 trials \times 15 observers). Numbers of trials with correct responses in the bare-finger, sheet, and lens conditions were 3, 24, and 49, respectively. The difference between the bare-finger and sheet conditions was highly significant, $p = 2.50 \times 10^{-6}$ by one-tailed Fisher's exact test. The difference between the sheet and lens conditions was also highly significant, $p = 2.48 \times 10^{-6}$ by one-tailed Fisher's exact test.

The increase in the accuracy from the bare-finger condition to the sheet condition is similar to Gordon and Cooper's [1975] findings. Lederman [1978] mentioned that the reduction of friction might improve the accuracy of detecting the presence of undulation. This may be a cause of the increase in the accuracy of detecting the position of a bump in our experiment. It is difficult to directly compare our results with Gordon and Cooper's results because the surfaces used in the experiments are different in overall shape (distribution of curvature) and stiffness.

The increase in the accuracy from the sheet condition to the lens condition does not seem to have any connection with previous reports. Because the bottom sides of the sheet and lens are covered with the same material (TFE film), the friction is unlikely to be concerned with this increase. Thus, this result suggests that the pins of the tactile contact lens have some effects that have not been reported. We present mathematical explanations of this phenomenon in section 3.

Although our results support the effectiveness of the device, more comprehensive experiments are needed. Our results are related specifically to the performance of detecting the position of a bump, not only to the performance of detecting the presence of a bump. This difference should be carefully considered in future experiments. The normal force and the speed of the finger's movement were not controlled or monitored in this experiment. Because the influence of these factors is considered homogeneous between the sheet and lens conditions, they are unlikely to be major causes of the difference between these two conditions. However, for a quantitative evaluation of the effectiveness of the tactile contact lens, the influence of these factors will need to be examined. Comparison between untrained observers and trained observers (such as craftworkers in the automobile industry) is also an interesting topic for future study.

3. THEORETICAL EXPLANATION

In this section, we provide a theoretical explanation of the effect of the tactile contact lens.

When the finger is moved over a target surface, the target surface geometry generates a spatio-temporal pattern of displacement on the skin surface. This results in spatio-temporal patterns of stress and strain in the skin tissue, and the mechanoreceptors translate them into neural signals. Electrophysiological studies

have shown that slowly adapting (SA) mechanoreceptive afferents respond to gradual steps stroked across the fingerpad [Lamotte and Srinivasan 1987]. This finding suggests that SA mechanoreceptors can play a major role in the detection of gradual undulations.

The purpose of this section is to clarify the physical mechanism of the sensitivity enhancing effect of the tactile contact lens. To this end, we aim to show the difference between the strain tensors in the presence and in the absence of the tactile contact lens. Because the strain tensor and stress tensor are dependent on each other, we focus only on the strain tensor in this paper. The role of mechanoreceptors, which translate the strain tensor into neural signals, is excluded from the consideration in this paper. This is because distinct difference in the strain tensor naturally results in difference in neural signals.

In this section, we first establish some assumptions to simplify the problem. We then derive the relation from the target surface geometry to the skin tissue strain. The mathematical expressions thus obtained suggest two possible explanations for the enhancing effect of the tactile contact lens: the lever-like behavior of the pins and the spatial aliasing effect caused by the discrete distribution of contact areas.

3.1 Assumptions

In order to build a simplified representation of the finger skin and the tactile contact lens, we use the following assumptions:

A1. The skin can be regarded as an incompressible, elastic halfspace (the Poisson's ratio, ν , is equal to $1/2$).

A2. The base sheet of the tactile contact lens always follows the geometry of the target surface, and does not lose touch with the target surface. Moreover, the pins of the tactile contact lens remain straight, perpendicular to the base sheet.

A3. There is no friction between the skin surface and the target surface, nor between the tactile contact lens and the target surface. However, the pins of the tactile contact lens always stick, without slipping, to the skin surface.

Some researchers have analyzed the strain and stress distributions in the finger skin. Numerical models using the finite element method have been used to analyze the roles of mechanoreceptors [Maeno et al. 1998; Dandekar et al. 2003]. Analytical methods based on the continuum mechanics theory [Fearing 1990; Phillips and Johnson 1981; Fearing and Hollerbach 1985] have also been used for the modeling of the finger skin, but these studies have been limited to two-dimensional modeling. Because the tactile contact lens provides point-like contact forces, a three-dimensional model is preferable in this case. The equations of the stress-strain-displacement relations in three-dimensional space are very complicated. However, as we show in this section, we can concisely formulate these relations by introducing the assumption $\nu = 1/2$ and using the frequency-domain approach.

Assumption *A1* ignores the presence of the bone beneath the skin. It is difficult to include the bone in the model because of the mathematical complexity, and because the effect of the skin tissue being compressed against the bone is still unclear. In similar circumstances, some researchers have used the two-dimensional halfplane assumption [Fearing 1990; Phillips and Johnson 1981]. Notably, Fearing [1990]

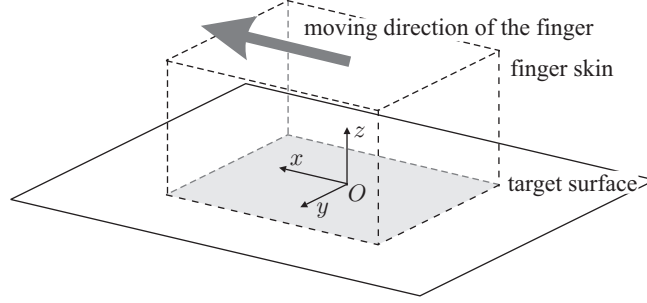


Fig. 3. The coordinate system.

found little difference in comparison of an elastic halfplane model and a model of an elastic layer with a rigid foundation. We therefore assume that the skin can be modeled as a halfspace. The non-linearity of the skin is ignored because when the target surface geometry is gradual enough, the deformation resulting from the surface geometry is limited to a small range.

This assumption also ignores the layered structure of the skin (composed of epidermis, dermis, and subcutis) and the epidermal ridges on the skin surface. This is because the purpose of our modeling is not to examine the roles of skin structures, but to clarify the difference between the presence and the absence of the tactile contact lens. Even if more complex models were built, it would be very difficult to draw useful insights from such complex models. Moreover, the remaining unmodeled structures and the physical differences among individuals may make such complex models meaningless.

Assumptions $A2$ and $A3$ are used in order to model an “ideal” tactile contact lens because our purpose is to clarify the mechanism of its effect. These assumptions may need to be reconsidered in future work for quantitative evaluation of real tactile contact lenses having finite stiffness and realistic friction coefficients. This topic is discussed in section 4.4.

3.2 Nomenclature

A = pin length, which is 3.5×10^{-3} m with the prototype.

$$\tilde{c}(\xi, \eta) = 1 - Z\sqrt{\xi^2 + \eta^2}.$$

\mathcal{F}_* = Fourier transform over the subscripted variable(s), e.g.,

$$\mathcal{F}_x[\phi(x)](\xi) = \int_{-\infty}^{\infty} \phi(x)e^{-j\xi x} dx.$$

\mathcal{F}_*^{-1} = inverse Fourier transform over the subscripted variable(s), e.g.,

$$\mathcal{F}_\xi^{-1}[\tilde{\phi}(\xi)](x) = \int_{-\infty}^{\infty} \tilde{\phi}(\xi)e^{j\xi x} d\xi / (2\pi).$$

$\tilde{\mathcal{G}}(\xi, \eta)$ = spatial-frequency response function from the surface displacement to the strain at depth Z .

$\tilde{g}(\xi, \eta)$ = spatial-frequency response function from $H(t, x, y)$ to $\varepsilon(t, x, y)$ in case with bare finger.

$h(x, y)$ = geometry of the target surface.

$$H(t, x, y) = h(x + Vt, y).$$

j = imaginary unit.

$J_k(\cdot)$ = k -th order Bessel function of the first kind.

$\tilde{\mathbf{k}}(x, y, \xi, \eta)$ = spatial-frequency response function from $H(t, x, y)$ to $\boldsymbol{\varepsilon}(t, x, y)$ in case with the tactile contact lens.

p, q = indices.

$$\tilde{r}(\xi, \eta) = \tilde{r}_o(\xi, \eta)/(4\pi P^2).$$

$r_o(x, y)$ = shape function of a single pin.

P = pin pitch $/(2\pi)$, which is 2.4×10^{-4} m with the prototype.

R = pin radius, which is 5.0×10^{-4} m with the prototype.

t = time.

$\mathbf{u}(t, x, y)$ = surface displacement of the finger skin.

V = the speed of finger's movement.

x, y = coordinate system parallel to the surface of the finger skin .

Z = mechanoreceptor depth, which is supposed to be approximately 5.0×10^{-4} to 1.0×10^{-3} m [Phillips and Johnson 1981].

\mathcal{Z}^2 = the set of all pairs of integers.

$\delta(\cdot)$ = Dirac delta function.

$\boldsymbol{\varepsilon}(t, x, y)$ = vector composed of the elements of the strain tensor at position (x, y) , depth Z .

ξ, η = spatial frequencies in x and y directions, respectively.

ω = temporal frequency.

\otimes_* = convolution with respect to the subscripted variable(s), e.g.,

$$\tilde{\phi}(\xi) \otimes_{\xi} \tilde{\psi}(\xi) = \int_{-\infty}^{\infty} \tilde{\phi}(\xi - \xi_1) \tilde{\psi}(\xi_1) d\xi_1$$

$$\phi(x, y) \otimes_{xy} \psi(x, y) = \int_{-\infty}^{\infty} \int_{-\infty}^{\infty} \phi(x - x_1, y - y_1) \psi(x_1, y_1) dx_1 dy_1.$$

$\tilde{*}(\xi, \eta)$ = the 2-dimensional Fourier transform of $*(x, y)$ over x and y if $*(x, y)$ is defined.

$\tilde{*}(\omega, \xi, \eta)$ = the 3-dimensional Fourier transform of $*(t, x, y)$ over $t, x,$ and y if $*(t, x, y)$ is defined.

$*_B, *_L$ = the case with bare finger and the case with tactile contact lens, respectively.

3.3 From target surface geometry to skin surface displacement

The information of the target surface geometry is transduced into the displacement on the skin surface. Here, we derive the relation between the target surface geometry and the skin surface displacement. The coordinate system is chosen as shown in Figure 3. Let the elevation of the target surface at position (x, y) be denoted by $h(x, y)$. Let the displacement of the skin surface at position (x, y) at time t be denoted by $\mathbf{u}(t, x, y) (\in \mathcal{R}^3)$. Assume that the target surface is moved at velocity $(-V, 0, 0)$ while the skin surface is fixed. This situation is equivalent to that where the skin is moved at velocity $(V, 0, 0)$ while the target surface is fixed.

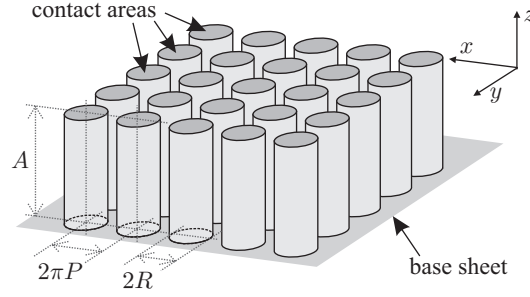


Fig. 4. The model of the tactile contact lens.

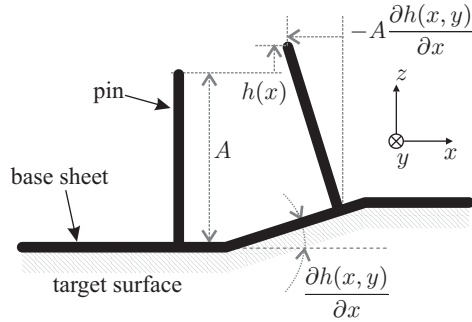


Fig. 5. Displacement of pin-tips caused by surface undulation.

When the skin surface is directly in touch with the target surface (i.e., in bare-finger touch), the displacement of the skin surface is determined by

$$\mathbf{u}_B(t, x, y) = h(x + Vt, y) [0 \ 0 \ 1]^T \quad (1)$$

if the assumption $A\mathcal{J}$ (no friction assumption) holds. Here, the subscript B indicates “bare finger.” The Fourier transform of $\mathbf{u}_B(t, x, y)$ is given as follows:

$$\tilde{\mathbf{u}}_B(\omega, \xi, \eta) = \frac{2\pi}{V} \tilde{h}\left(\frac{\omega}{V}, \eta\right) \delta\left(\xi - \frac{\omega}{V}\right) [0 \ 0 \ 1]^T, \quad (2)$$

where $\tilde{h}(\xi, \eta)$ is the Fourier transform of $h(x, y)$. Let us define

$$\tilde{H}(\omega, \xi, \eta) = \mathcal{F}_{txy}[h(x + Vt, y)](\omega, \xi, \eta) = \frac{2\pi}{V} \tilde{h}\left(\frac{\omega}{V}, \eta\right) \delta\left(\xi - \frac{\omega}{V}\right). \quad (3)$$

Then, $\tilde{\mathbf{u}}_B(\omega, \xi, \eta)$ can be simply rewritten as

$$\tilde{\mathbf{u}}_B(\omega, \xi, \eta) = \tilde{H}(\omega, \xi, \eta) [0 \ 0 \ 1]^T. \quad (4)$$

When the tactile contact lens is used, the displacement distribution on the skin surface is more complex. We model the tactile contact lens as illustrated in Figure 4. In this model, the pins are cylinders of radius R and length A , and are arranged at a pitch of $2\pi P$. Because the inter-pin separation becomes $2(\pi P - R)$, P and

R satisfy $R < \pi P$. Based on this model, the contact area on the skin surface is described by the following function $m(x, y)$:

$$m(x, y) = \sum_{\{p, q\} \in \mathcal{Z}^2} r_o(x - 2\pi Pp, y - 2\pi Pq), \quad (5)$$

where

$$r_o(x, y) = \begin{cases} 1, & \text{if } x^2 + y^2 < R^2 \\ 0, & \text{otherwise.} \end{cases} \quad (6)$$

Here, \mathcal{Z}^2 denotes the set of all pairs of integers. Because $R < \pi P$, $m(x, y)$ takes the values of either 1 or 0. The contact area is the set of points (x, y) for which $m(x, y) = 1$. Let us assume that the skin surface is displaced only in the contact area, and the surface geometry is band-limited to low (spatial) frequencies compared to $1/R$. Then, in the contact area, the normal displacement of the skin surface is determined by the target surface elevation $h(x, y)$. On the other hand, as shown in Figure 5, the tangential displacement is determined by the angle of the pins, which is determined by the inclination of the target surface. That is, the surface displacement is described as

$$\mathbf{u}_L(t, x, y) = \mathbf{s}(x + Vt, y)m(x, y), \quad (7)$$

where

$$\mathbf{s}(x, y) = \left[-A \frac{\partial h(x, y)}{\partial x}, -A \frac{\partial h(x, y)}{\partial y}, h(x, y) \right]^T \quad (8)$$

and the subscript L denotes ‘‘lens.’’

The Fourier transform of $\mathbf{s}(x, y)$ is written as

$$\tilde{\mathbf{s}}(\xi, \eta) = \tilde{h}(\xi, \eta) \begin{bmatrix} -jA\xi & -jA\eta & 1 \end{bmatrix}^T, \quad (9)$$

and that of $m(x, y)$ is written as

$$\begin{aligned} \tilde{m}(\xi, \eta) &= \sum_{\{p, q\} \in \mathcal{Z}^2} e^{2\pi j P(p\xi + q\eta)} \tilde{r}_o(\xi, \eta) \\ &= \sum_{\{p, q\} \in \mathcal{Z}^2} \delta(P\xi - p) \delta(P\eta - q) \tilde{r}_o(\xi, \eta) \\ &= \frac{1}{P^2} \sum_{\{p, q\} \in \mathcal{Z}^2} \tilde{r}_o\left(\frac{p}{P}, \frac{q}{P}\right) \delta\left(\xi - \frac{p}{P}\right) \delta\left(\eta - \frac{q}{P}\right), \end{aligned} \quad (10)$$

where j is the imaginary unit, $\delta(\cdot)$ is the Dirac delta function, and $\tilde{r}_o(\xi, \eta)$ is the Fourier transform of $r_o(x, y)$. Function $\tilde{r}_o(\xi, \eta)$ can be derived as follows:

$$\begin{aligned} \tilde{r}_o(\xi, \eta) &= \int_{-\infty}^{\infty} \int_{-\infty}^{\infty} r_o(x, y) e^{-j(x\xi + y\eta)} dx dy \\ &= \int_0^R \int_0^{2\pi} e^{-jr\rho(\cos\phi \cos\theta + \sin\phi \sin\theta)} r d\theta dr \\ &= \int_0^R 2\pi r J_0(r\rho) dr \end{aligned}$$

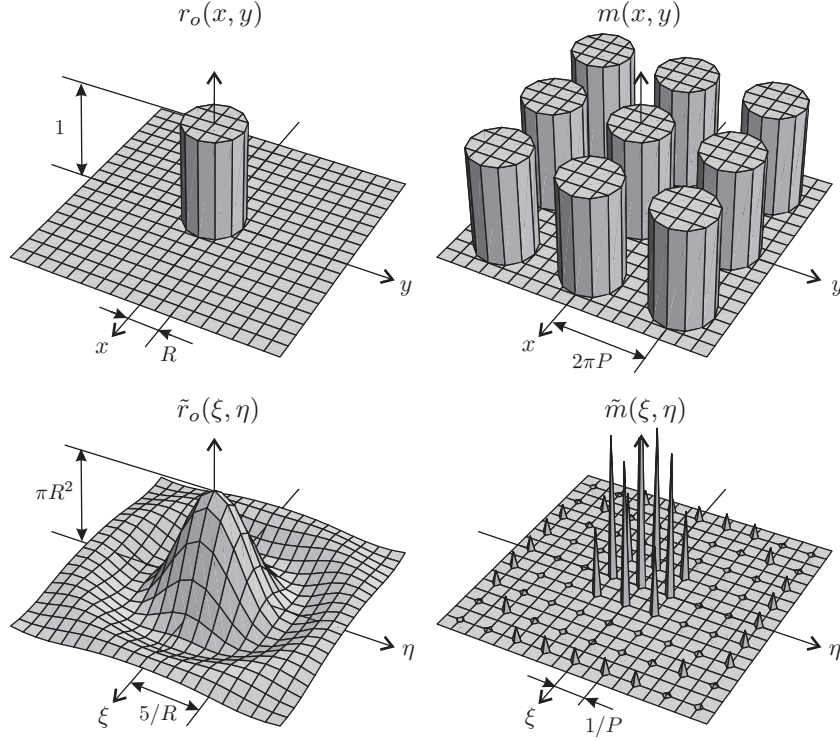


Fig. 6. Plots of functions $r_o(x, y)$, $m(x, y)$, $\tilde{r}_o(\xi, \eta)$, and $\tilde{m}(\xi, \eta)$. Function $r_o(x, y)$ represents the contact with a single pin, and function $m(x, y)$ represents that with an array of pins. Functions $\tilde{r}_o(\xi, \eta)$ and $\tilde{m}(\xi, \eta)$ are the Fourier transforms of $r_o(x, y)$ and $m(x, y)$, respectively.

$$= \frac{2\pi R J_1(R\sqrt{\xi^2 + \eta^2})}{\sqrt{\xi^2 + \eta^2}}, \quad (11)$$

where $\rho = \sqrt{\xi^2 + \eta^2}$, $r = \sqrt{x^2 + y^2}$, $J_k(\cdot)$ is the k -th order Bessel function of the first kind. Here, we used the following properties of the Bessel functions [Bowman 1958]:

$$\int_0^{2\pi} e^{ja \cos \theta} d\theta = 2\pi J_0(a), \quad \int_0^b x J_0(ax) dx = \frac{b}{a} J_1(ab).$$

Figure 6 shows plots of functions $r_o(x, y)$, $m(x, y)$, $\tilde{r}_o(\xi, \eta)$, and $\tilde{m}(\xi, \eta)$.

Using $\tilde{\mathbf{s}}(\xi, \eta)$ and $\tilde{m}(\xi, \eta)$, we can derive the Fourier transform of $\mathbf{u}_L(t, x, y)$. Noting that a multiplication in xy -space is equivalent to a convolution in $\xi\eta$ -space, we can derive the Fourier transform of $\mathbf{u}_L(t, x, y)$ over x and y as follows:

$$\mathcal{F}_{xy}[\mathbf{u}_L(t, x, y)](\xi, \eta) = \frac{1}{4\pi^2} (e^{jV\xi t} \tilde{\mathbf{s}}(\xi, \eta)) \otimes_{\xi\eta} \tilde{m}(\xi, \eta), \quad (12)$$

where $\otimes_{\xi\eta}$ denotes the convolution over ξ and η . The 3-dimensional Fourier transform of $\mathbf{u}(t, x, y)$ over t , x , and y is obtained as the Fourier transform of (12) over

t. This is written as

$$\begin{aligned}
\tilde{\mathbf{u}}_L(\omega, \xi, \eta) &= \frac{1}{4\pi^2} \int_{-\infty}^{\infty} e^{-j\omega t} \left((e^{jV\xi t} \tilde{\mathbf{s}}(\xi, \eta)) \otimes_{\xi\eta} \tilde{m}(\xi, \eta) \right) dt \\
&= \frac{1}{4\pi^2} \int_{-\infty}^{\infty} \int_{-\infty}^{\infty} \int_{-\infty}^{\infty} e^{j(V\xi_1 - \omega)t} \tilde{\mathbf{s}}(\xi_1, \eta_1) \tilde{m}(\xi - \xi_1, \eta - \eta_1) d\xi_1 d\eta_1 dt \\
&= \frac{1}{2\pi V} \int_{-\infty}^{\infty} \int_{-\infty}^{\infty} \delta\left(\xi_1 - \frac{\omega}{V}\right) \tilde{\mathbf{s}}(\xi_1, \eta_1) \tilde{m}(\xi - \xi_1, \eta - \eta_1) d\xi_1 d\eta_1 \\
&= \frac{1}{2\pi V} \int_{-\infty}^{\infty} \tilde{\mathbf{s}}\left(\frac{\omega}{V}, \eta_1\right) \tilde{m}\left(\xi - \frac{\omega}{V}, \eta - \eta_1\right) d\eta_1 \\
&= \frac{1}{2\pi V} \tilde{\mathbf{s}}\left(\frac{\omega}{V}, \eta\right) \otimes_{\eta} \tilde{m}\left(\xi - \frac{\omega}{V}, \eta\right) \\
&= \frac{1}{2\pi V P^2} \begin{bmatrix} -jA\xi \\ -jA\eta \\ 1 \end{bmatrix} \sum_{\{p,q\} \in \mathcal{Z}^2} \tilde{r}_o\left(\frac{p}{P}, \frac{q}{P}\right) \tilde{h}\left(\frac{\omega}{V}, \eta - \frac{q}{P}\right) \delta\left(\xi - \frac{\omega}{V} - \frac{p}{P}\right). \quad (13)
\end{aligned}$$

For simplicity of further considerations, let us define

$$\tilde{r}(\xi, \eta) = \frac{\tilde{r}_o(\xi, \eta)}{4\pi^2 P^2} = \frac{R J_1(R\sqrt{\xi^2 + \eta^2})}{2\pi P^2 \sqrt{\xi^2 + \eta^2}}. \quad (14)$$

Then, $\tilde{\mathbf{u}}_L(\omega, \xi, \eta)$ is rewritten as

$$\tilde{\mathbf{u}}_L(\omega, \xi, \eta) = \frac{2\pi}{V} \begin{bmatrix} -jA\xi \\ -jA\eta \\ 1 \end{bmatrix} \sum_{\{p,q\} \in \mathcal{Z}^2} \tilde{r}\left(\frac{p}{P}, \frac{q}{P}\right) \tilde{h}\left(\frac{\omega}{V}, \eta - \frac{q}{P}\right) \delta\left(\xi - \frac{\omega}{V} - \frac{p}{P}\right). \quad (15)$$

Using $H(\omega, \xi, \eta)$, which is defined in (3), we can further simplify $\tilde{\mathbf{u}}_L(\omega, \xi, \eta)$ as

$$\tilde{\mathbf{u}}_L(\omega, \xi, \eta) = \begin{bmatrix} -jA\xi \\ -jA\eta \\ 1 \end{bmatrix} \sum_{\{p,q\} \in \mathcal{Z}^2} \tilde{r}\left(\frac{p}{P}, \frac{q}{P}\right) \tilde{H}\left(\omega, \xi - \frac{p}{P}, \eta - \frac{q}{P}\right). \quad (16)$$

We have to note that $\tilde{r}(0, 0) = R^2/(4\pi P^2)$, which is equal to the ratio of the contact area to the total area, $(\pi R^2)/(2\pi P)^2$. Because $R < \pi P$, we have $\tilde{r}(0, 0) < \pi/4$.

Equation (16) can be seen to represent the aliasing effect in the spatial frequency domain. This is caused by the discrete distribution of contact areas on the skin surface. Figure 7 shows a schematic representation of this effect. By the aliasing effect, $\tilde{H}(\omega, \xi, \eta)$ is duplicated at a regular interval $1/P$ in $\xi\eta$ -space. As seen in (16), the duplicated information, $\tilde{H}(\omega, \xi - p/P, \eta - q/P)$, is scaled by the coefficient $\tilde{r}(p/P, q/P)$. The plot of $\tilde{r}_o(\xi, \eta)$ in Figure 6 and the definition of $\tilde{r}(\xi, \eta)$ in (14) imply that a large value of R provides function $\tilde{r}(\xi, \eta)$ with a high and narrow peak at $\xi = \eta = 0$. This results in small values of $\tilde{r}(p/P, q/P)$ where $p \neq 0$ or $q \neq 0$. That is, as the radius of the pins becomes larger, the impact of the aliasing effect becomes smaller.

3.4 From skin surface displacement to skin tissue strain

Next, we derive the relation between the skin surface displacement and the skin tissue strain. The skin surface displacement results from the force distributed over the

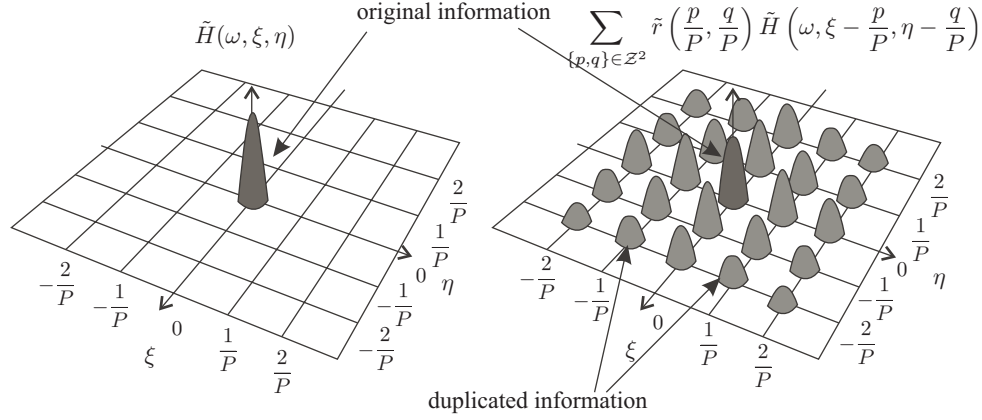


Fig. 7. Schematic of the spatial aliasing effect.

skin surface. The relation between the surface force and the surface displacement and the relation between the surface force and the strain can be derived by using the theory of elasticity. By using these relations, we derive the spatial-frequency response function that relates the surface displacement to the strain.

Now assume that a concentrated force \mathbf{F} ($\in \mathcal{R}^3$) is applied to the position $(0, 0)$ on the surface, and let $\mathbf{u}_1(x, y, z)$ ($\in \mathcal{R}^3$) be the displacement at position (x, y) , depth z . The relation between \mathbf{F} and $\mathbf{u}_1(x, y, z)$ has been known since the nineteenth century [Love 1927]. Although this relation has a complicated form, setting $\nu = 1/2$ yields a simpler expression: $\mathbf{u}_1(x, y, z) = \mathbf{K}(x, y, z)\mathbf{F}$, where

$$\mathbf{K}(x, y, z) = \frac{3}{4\pi E(x^2 + y^2 + z^2)^{3/2}} \begin{bmatrix} 2x^2 + y^2 + z^2 & xy & xz \\ xy & x^2 + 2y^2 + z^2 & yz \\ xz & yz & x^2 + y^2 + 2z^2 \end{bmatrix}.$$

Here, E is the Young's modulus. This relation can be easily expanded into the case with distributed surface force. Let $\mathbf{f}_o(x, y)$ ($\in \mathcal{R}^3$) be the surface traction (surface force per unit area) at position (x, y) . Then, according to the principle of superposition, $\mathbf{f}_o(x, y)$ and $\mathbf{u}_1(x, y, z)$ are connected by $\mathbf{u}_1(x, y, z) = \mathbf{K}(x, y, z) \otimes_{xy} \mathbf{f}_o(x, y)$, where \otimes_{xy} denotes the convolution with respect to x and y .

Let $\mathbf{u}_o(x, y)$ ($\in \mathcal{R}^3$) be the surface displacement at position (x, y) , and let $\boldsymbol{\varepsilon}_o(x, y) = [\varepsilon_{xx}, \varepsilon_{yy}, \varepsilon_{zz}, \varepsilon_{xy}, \varepsilon_{yz}, \varepsilon_{zx}]^T$ ($\in \mathcal{R}^6$) be the strain at position (x, y) , depth Z . (Hereafter, we treat Z as a constant.) Then, $\mathbf{u}_o(x, y)$ is obtained by setting $z = 0$ in $\mathbf{u}_1(x, y, z)$, and $\boldsymbol{\varepsilon}_o(x, y)$ is obtained by the first-order spatial derivative of $\mathbf{u}_1(x, y, z)$. Thus, the relations among $\mathbf{u}_o(x, y)$, $\mathbf{f}_o(x, y)$, and $\boldsymbol{\varepsilon}_o(x, y)$ are described as follows:

$$\mathbf{u}_o(x, y) = \mathbf{K}_{uf}(x, y) \otimes_{xy} \mathbf{f}_o(x, y), \quad (17)$$

$$\boldsymbol{\varepsilon}_o(x, y) = \mathbf{K}_{\varepsilon f}(x, y) \otimes_{xy} \mathbf{f}_o(x, y), \quad (18)$$

where

$$\mathbf{K}_{uf}(x, y) = \frac{3}{4\pi E(x^2 + y^2)^{3/2}} \begin{bmatrix} 2x^2 + y^2 & xy & 0 \\ xy & x^2 + 2y^2 & 0 \\ 0 & 0 & x^2 + y^2 \end{bmatrix},$$

$$\mathbf{K}_{\varepsilon f}(x, y) = \frac{3}{4\pi E(x^2 + y^2 + Z^2)^{5/2}} \begin{bmatrix} -2x^2 + y^2 + Z^2 \\ x^2 - 2y^2 + Z^2 \\ x^2 + y^2 - 2Z^2 \\ -6xy \\ -6Zy \\ -6Zx \end{bmatrix} [x \ y \ Z].$$

The spatial frequency-domain representations of relations (17) and (18) are respectively written as

$$\tilde{\mathbf{u}}_o(\xi, \eta) = \tilde{\mathbf{K}}_{uf}(\xi, \eta) \tilde{\mathbf{f}}_o(\xi, \eta), \quad (19)$$

$$\tilde{\boldsymbol{\varepsilon}}_o(\xi, \eta) = \tilde{\mathbf{K}}_{\varepsilon f}(\xi, \eta) \tilde{\mathbf{f}}_o(\xi, \eta), \quad (20)$$

where

$$\tilde{\mathbf{K}}_{uf}(\xi, \eta) = \frac{3}{2E\rho^3} \begin{bmatrix} \rho^2 + \eta^2 & -\xi\eta & 0 \\ -\xi\eta & \rho^2 + \xi^2 & 0 \\ 0 & 0 & \rho^2 \end{bmatrix},$$

$$\tilde{\mathbf{K}}_{\varepsilon f}(\xi, \eta) = \frac{3e^{-Z\rho}}{2E\rho^3} \begin{bmatrix} j\xi(\xi^2(1-Z\rho) + 2\eta^2) & -j\xi^2\eta(1+Z\rho) & Z\rho^2\xi^2 \\ -j\xi\eta^2(1+Z\rho) & j\eta(2\xi^2 + \eta^2(1-Z\rho)) & Z\rho^2\eta^2 \\ -j\rho^2\xi(1-Z\rho) & -j\rho^2\eta(1-Z\rho) & -Z\rho^4 \\ 2Z\rho^2\xi\eta & 2\rho^2(Z\eta^2 - \rho) & 2jZ\rho^3\eta \\ 2\rho^2(Z\xi^2 - \rho) & 2Z\rho^2\xi\eta & 2jZ\rho^3\xi \\ 2j\eta(\eta^2 - Z\rho\xi^2) & 2j\xi(\xi^2 - Z\rho\eta^2) & 2Z\rho^2\xi\eta \end{bmatrix},$$

and $\rho = \sqrt{\xi^2 + \eta^2}$. The appendix presents the details of the derivations.

Using (19) and (20), we can connect $\mathbf{u}_o(x, y)$ and $\boldsymbol{\varepsilon}_o(x, y)$ by

$$\tilde{\boldsymbol{\varepsilon}}_o(\xi, \eta) = \tilde{\mathbf{G}}(\xi, \eta) \tilde{\mathbf{u}}_o(\xi, \eta), \quad (21)$$

where

$$\begin{aligned} \tilde{\mathbf{G}}(\xi, \eta) &= \tilde{\mathbf{K}}_{\varepsilon f}(\xi, \eta) \tilde{\mathbf{K}}_{uf}(\xi, \eta)^{-1} \\ &= \frac{e^{-Z\rho}}{\rho} \begin{bmatrix} -j\xi(Z\xi^2 - \rho) & -jZ\xi^2\eta & Z\rho\xi^2 \\ -jZ\xi\eta^2 & -j\eta(Z\eta^2 - \rho) & Z\rho\eta^2 \\ -j\rho\xi(1-Z\rho) & -j\rho\eta(1-Z\rho) & -Z\rho^3 \\ -\xi\eta(1-2Z\rho) & -\xi^2 - 2\eta^2(1-Z\rho) & 2jZ\rho^2\eta \\ -\eta^2 - 2\xi^2(1-Z\rho) & -\xi\eta(1-2Z\rho) & 2jZ\rho^2\xi \\ -j\eta(2Z\xi^2 - \rho) & -j\xi(2Z\eta^2 - \rho) & 2Z\rho\xi\eta \end{bmatrix}. \end{aligned} \quad (22)$$

Thus, we obtain $\tilde{\mathbf{G}}(\xi, \eta)$, the spatial-frequency response function from the skin surface displacement to the skin tissue strain.

3.5 From target surface geometry to skin tissue strain

By using the derived results in sections 3.3 and 3.4, we derive the spatio-temporal distribution of strain, $\boldsymbol{\varepsilon}(t, x, y)$, and its Fourier transform, $\tilde{\boldsymbol{\varepsilon}}(\omega, \xi, \eta)$. Simply ex-

panding relation (21) into $\omega\xi\eta$ -space yields

$$\tilde{\mathbf{e}}(\omega, \xi, \eta) = \tilde{\mathbf{G}}(\xi, \eta)\tilde{\mathbf{u}}(\omega, \xi, \eta), \quad (23)$$

where $\tilde{\mathbf{u}}(\omega, \xi, \eta)$ is the spatio-temporal pattern of surface displacement derived in section 3.3. By substituting (23) by (4), we can express $\tilde{\mathbf{e}}(\omega, \xi, \eta)$ in the case with bare finger as follows:

$$\tilde{\mathbf{e}}_B(\omega, \xi, \eta) = \tilde{\mathbf{g}}(\xi, \eta)\tilde{H}(\omega, \xi, \eta), \quad (24)$$

where $\tilde{\mathbf{g}}(\xi, \eta)$ is the third column vector of $\tilde{\mathbf{G}}(\xi, \eta)$, which is written as

$$\tilde{\mathbf{g}}(\xi, \eta) = Ze^{-Z\rho} [\xi^2, \eta^2, -\rho^2, 2j\rho\eta, 2j\rho\xi, 2\xi\eta]^T. \quad (25)$$

On the other hand, by substituting (23) by (16), $\tilde{\mathbf{e}}(\omega, \xi, \eta)$ in the case with the tactile contact lens is obtained as

$$\tilde{\mathbf{e}}_L(\omega, \xi, \eta) = \sum_{\{p,q\} \in \mathcal{Z}^2} \tilde{r}\left(\frac{p}{P}, \frac{q}{P}\right) \tilde{\mathbf{G}}(\xi, \eta) \begin{bmatrix} -jA\xi \\ -jA\eta \\ 1 \end{bmatrix} \tilde{H}\left(\omega, \xi - \frac{p}{P}, \eta - \frac{q}{P}\right). \quad (26)$$

From the definition of $\tilde{\mathbf{G}}(\xi, \eta)$ in (22), the following identity holds true:

$$\tilde{\mathbf{G}}(\xi, \eta) \begin{bmatrix} -j\xi \\ -j\eta \\ 0 \end{bmatrix} = \left(\frac{1}{Z} - \sqrt{\xi^2 + \eta^2}\right) \tilde{\mathbf{G}}(\xi, \eta) \begin{bmatrix} 0 \\ 0 \\ 1 \end{bmatrix}. \quad (27)$$

By using this, we can rewrite $\tilde{\mathbf{e}}_L(\omega, \xi, \eta)$ as

$$\tilde{\mathbf{e}}_L(\omega, \xi, \eta) = \sum_{\{p,q\} \in \mathcal{Z}^2} \tilde{r}\left(\frac{p}{P}, \frac{q}{P}\right) \left(\frac{A}{Z}\tilde{c}(\xi, \eta) + 1\right) \tilde{\mathbf{g}}(\xi, \eta)\tilde{H}\left(\omega, \xi - \frac{p}{P}, \eta - \frac{q}{P}\right), \quad (28)$$

where

$$\tilde{c}(\xi, \eta) = 1 - Z\sqrt{\xi^2 + \eta^2}. \quad (29)$$

Moreover, by letting

$$\tilde{\gamma}_{pq}(\xi, \eta) = \tilde{r}\left(\frac{p}{P}, \frac{q}{P}\right) \left(\frac{A}{Z}\tilde{c}\left(\xi + \frac{p}{P}, \eta + \frac{q}{P}\right) + 1\right) \tilde{\mathbf{g}}\left(\xi + \frac{p}{P}, \eta + \frac{q}{P}\right), \quad (30)$$

$\tilde{\mathbf{e}}_L(\omega, \xi, \eta)$ can be further rewritten as

$$\tilde{\mathbf{e}}_L(\omega, \xi, \eta) = \sum_{\{p,q\} \in \mathcal{Z}^2} \tilde{\gamma}_{pq}\left(\xi - \frac{p}{P}, \eta - \frac{q}{P}\right) \tilde{H}\left(\omega, \xi - \frac{p}{P}, \eta - \frac{q}{P}\right). \quad (31)$$

For convenience of comparison between $\tilde{\mathbf{e}}_B(\omega, \xi, \eta)$ and $\tilde{\mathbf{e}}_L(\omega, \xi, \eta)$, we respectively rewrite (24) and (31) as follows:

$$\mathcal{F}_{\xi\eta}^{-1}[\tilde{\mathbf{e}}_B(\omega, \xi, \eta)](x, y) = \mathcal{F}_{\xi\eta}^{-1}[\tilde{\mathbf{g}}(\xi, \eta)\tilde{H}(\omega, \xi, \eta)](x, y), \quad (32)$$

$$\mathcal{F}_{\xi\eta}^{-1}[\tilde{\mathbf{e}}_L(\omega, \xi, \eta)](x, y) = \mathcal{F}_{\xi\eta}^{-1}[\tilde{\mathbf{k}}(x, y, \xi, \eta)\tilde{H}(\omega, \xi, \eta)](x, y), \quad (33)$$

where

$$\tilde{\mathbf{k}}(x, y, \xi, \eta) = \sum_{\{p,q\} \in \mathcal{Z}^2} e^{j\left(\frac{p}{P}x + \frac{q}{P}y\right)} \tilde{\gamma}_{pq}(\xi, \eta). \quad (34)$$

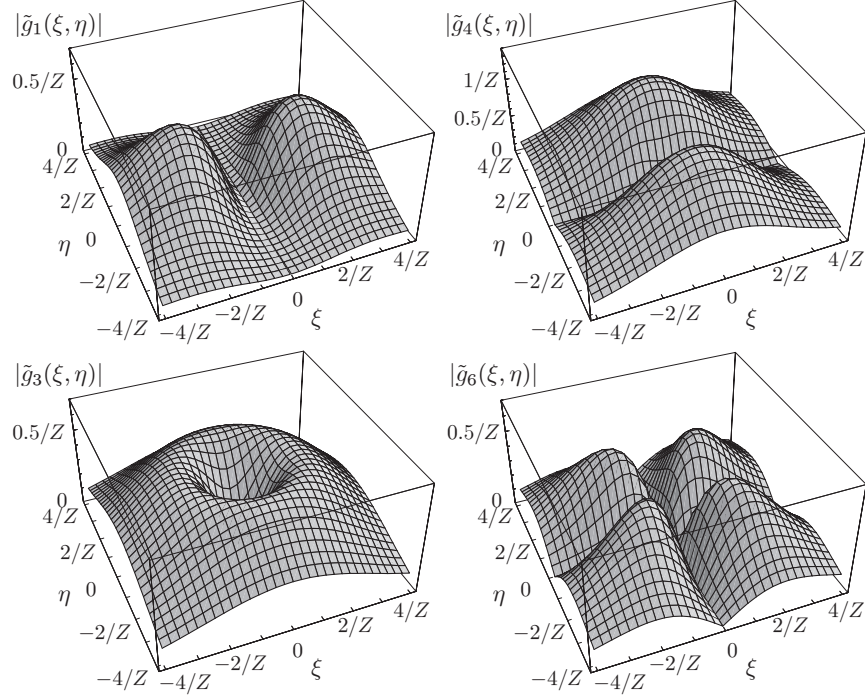


Fig. 8. Plots of functions $|\tilde{g}_i(\xi, \eta)|$, $i = 1, 3, 4$, and 6 . Plots of $|\tilde{g}_2(\xi, \eta)|$ and $|\tilde{g}_5(\xi, \eta)|$ are not shown, but can be obtained by switching ξ - and η -axes of $|\tilde{g}_1(\xi, \eta)|$'s and $|\tilde{g}_3(\xi, \eta)|$'s plots, respectively. A spatial frequency vector $[\xi, \eta]$ at which $|\tilde{g}_i(\xi, \eta)|$ is maximum satisfies $\sqrt{\xi^2 + \eta^2} = 2/Z$.

From (32) and (33), we can see that $\tilde{\mathbf{g}}(\xi, \eta)$ and $\tilde{\mathbf{k}}(x, y, \xi, \eta)$ are the frequency response functions from the surface geometry, $\tilde{H}(\omega, \xi, \eta)$, to the strain, $\tilde{\boldsymbol{\varepsilon}}(\omega, \xi, \eta)$, in the case with bare finger and in the case with the tactile contact lens, respectively. We have to note that $\tilde{\mathbf{k}}(x, y, \xi, \eta)$ is dependent on (x, y) . This is because the temporal change in the strain at position (x, y) is dependent on the positional relationship between position (x, y) and the contact areas (i.e., the pin-tips).

3.6 Physical meanings

The reasons for the magnifying effect caused by the tactile contact lens can be seen from the comparison between $\tilde{\mathbf{g}}(\xi, \eta)$ and $\tilde{\mathbf{k}}(x, y, \xi, \eta)$. We can decompose $\tilde{\mathbf{k}}(x, y, \xi, \eta)$ into two terms:

$$\tilde{\mathbf{k}}(x, y, \xi, \eta) = \tilde{\mathbf{a}}(\xi, \eta)\tilde{\mathbf{g}}(\xi, \eta) + \tilde{\mathbf{b}}(x, y, \xi, \eta), \quad (35)$$

where

$$\tilde{\mathbf{a}}(\xi, \eta) = \tilde{r}(0, 0) \left(\frac{A}{Z}\tilde{c}(\xi, \eta) + 1 \right) = \frac{R^2}{4\pi P^2} \left(\frac{A}{Z} - A\sqrt{\xi^2 + \eta^2} + 1 \right) \quad (36)$$

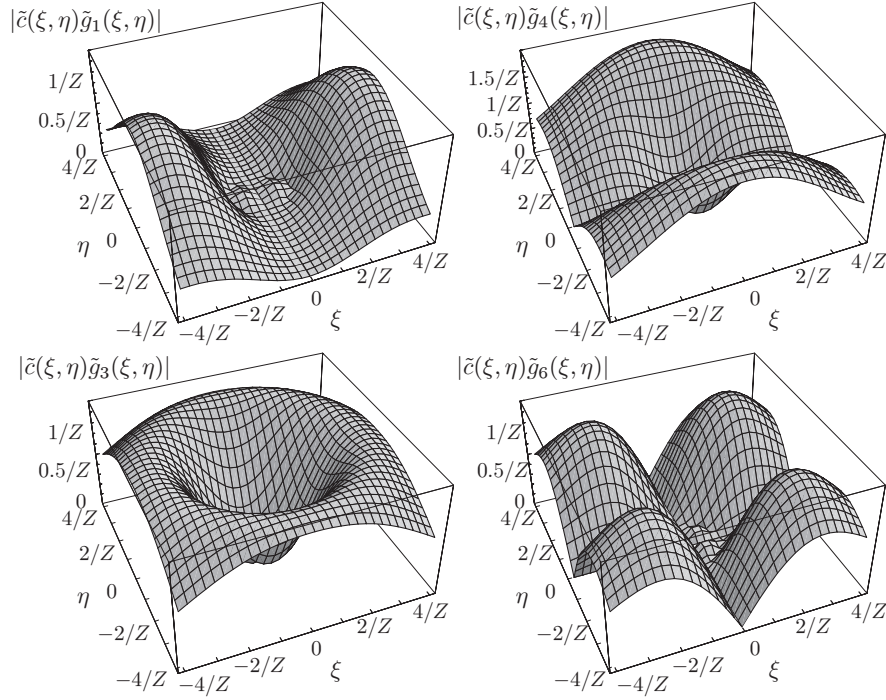


Fig. 9. Plots of functions $|\tilde{c}(\xi, \eta)\tilde{g}_i(\xi, \eta)|$, $i = 1, 3, 4$, and 6 . Plots of $|\tilde{c}(\xi, \eta)\tilde{g}_2(\xi, \eta)|$ and $|\tilde{c}(\xi, \eta)\tilde{g}_5(\xi, \eta)|$ are not shown, but can be obtained by switching ξ - and η -axes of $|\tilde{c}(\xi, \eta)\tilde{g}_1(\xi, \eta)|$'s and $|\tilde{c}(\xi, \eta)\tilde{g}_3(\xi, \eta)|$'s plots, respectively. A spatial frequency vector $[\xi, \eta]$ at which $|\tilde{c}(\xi, \eta)\tilde{g}_i(\xi, \eta)|$ is maximum satisfies $\sqrt{\xi^2 + \eta^2} = (2 + \sqrt{2})/Z$.

and

$$\begin{aligned}
 \tilde{\mathbf{b}}(x, y, \xi, \eta) &= \sum_{\{p, q\} \in \mathbb{Z}^2 \setminus \{0, 0\}} e^{j(\frac{p}{P}x + \frac{q}{P}y)} \tilde{\gamma}_{pq}(\xi, \eta) \\
 &= \sum_{\{p, q\} \in \mathbb{Z}^2 \setminus \{0, 0\}} e^{j(\frac{p}{P}x + \frac{q}{P}y)} \tilde{r}\left(\frac{p}{P}, \frac{q}{P}\right) \left(\tilde{\mathbf{g}}\left(\xi + \frac{p}{P}, \eta + \frac{q}{P}\right) \right. \\
 &\quad \left. + \frac{A}{Z} \tilde{c}\left(\xi + \frac{p}{P}, \eta + \frac{q}{P}\right) \tilde{\mathbf{g}}\left(\xi + \frac{p}{P}, \eta + \frac{q}{P}\right) \right). \quad (37)
 \end{aligned}$$

The first term of (35), $\tilde{a}(\xi, \eta)\tilde{\mathbf{g}}(\xi, \eta)$, represents the magnification of the strain tensor by a scalar factor $\tilde{a}(\xi, \eta)$. This effect is induced by the lever-like behavior of the pins, which converts the local inclination of the target surface into tangential displacement on the skin surface, as shown in Figure 5. It might be considered unnatural that the tangential displacement (caused by the pins) generates a magnified sensation of the normal displacement (produced in bare-finger touch). An explanation for this is provided by (27), which implies that the normal displacement distribution $\mathbf{u}(x, y) = [0, 0, u_z(x, y)]$ and the tangential displacement distribution $\mathbf{u}(x, y) = [-Z\partial u_z(x, y)/\partial x, -Z\partial u_z(x, y)/\partial y, 0]$ make an equivalent contribution to

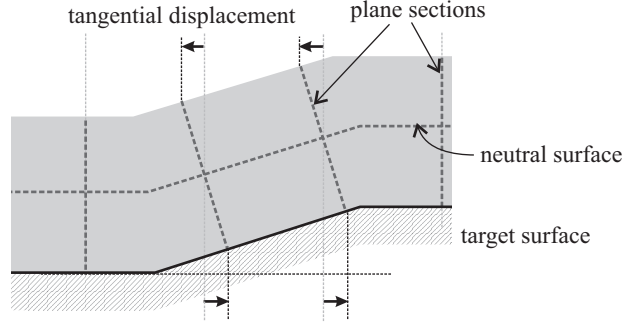


Fig. 10. Tangential displacement caused by the lever-effect of a flexible sheet of uniform thickness.

the strain tensor if $u_z(x, y)$ is band-limited to frequencies sufficiently smaller than $1/Z$.

The second term of (35), $\tilde{\mathbf{b}}(x, y, \xi, \eta)$, represents the aliasing effect, which is caused by the discrete distribution of the contact areas. Carefully looking at (37), we can see that this term can also operate to magnify the tactile stimuli. Let $\tilde{g}_i(\xi, \eta)$ ($i = 1, \dots, 6$) denote the elements of $\tilde{\mathbf{g}}(\xi, \eta)$. Seeing that (37) contains $\tilde{\mathbf{g}}(\xi, \eta)$ and $\tilde{c}(\xi, \eta)\tilde{\mathbf{g}}(\xi, \eta)$, we show plots of $|\tilde{g}_i(\xi, \eta)|$ and $|\tilde{c}(\xi, \eta)\tilde{g}_i(\xi, \eta)|$ in Figure 8 and Figure 9, respectively. As seen in these figures, every element of $\tilde{\mathbf{g}}(\xi, \eta)$ and $\tilde{c}(\xi, \eta)\tilde{\mathbf{g}}(\xi, \eta)$ has a band-pass filtering characteristic. Therefore, in the low frequency region ($\sqrt{\xi^2 + \eta^2} < 1/Z$, for example), $\tilde{g}_i(\xi + p/P, \eta + q/P)$ and $\tilde{c}(\xi + p/P, \eta + q/P)\tilde{g}_i(\xi + p/P, \eta + q/P)$ (appearing in (37)) can have a higher gain than $\tilde{g}_i(\xi, \eta)$ has. The factor A/Z , which multiplies $\tilde{c}(\xi + p/P, \eta + q/P)\tilde{\mathbf{g}}(\xi + p/P, \eta + q/P)$ in (37), also operates to magnify the strain. Thus, as a whole, the gain of $\tilde{\mathbf{b}}(x, y, \xi, \eta)$ can be large compared to the gain of $\tilde{\mathbf{g}}(\xi, \eta)$.

In summary, the above analysis suggests two explanations for the enhancing effect of the tactile contact lens. One is a lever-like behavior of the pins, which produces tangential skin surface displacement according to the local inclination of the target surface. The analysis shows that the strain caused by the tangential displacement produced by the pins is a magnification of the strain caused by the normal displacement produced in bare-finger touch. The second explanation is the spatial aliasing effect, which is caused by the discrete contact. This effect generates high spatial-frequency components in the skin surface displacement. Thus, the temporal change in the skin surface displacement is efficiently transduced into the temporal change in the skin tissue strain because incompressible elastic material (in this case, the skin) is a spatial band-pass filter when it is viewed as a transducer from surface displacement to strain.

4. DISCUSSION

4.1 Other sensitivity-enhancing materials

The analysis described in section 3 implies that even a flexible sheet of uniform thickness can improve the haptic detection of surface undulation. In this case, since the contact between the sheet and the finger skin is continuous, the second

term of (35) vanishes. To be more precise, the description of this case can be obtained by substituting

$$\tilde{\mathbf{u}}_U(\omega, \xi, \eta) = \begin{bmatrix} -jA\xi \\ -jA\eta \\ 1 \end{bmatrix} \tilde{H}(\omega, \xi, \eta), \quad (38)$$

$$\mathcal{F}_{\xi\eta}^{-1}[\tilde{\boldsymbol{\varepsilon}}_U(\omega, \xi, \eta)](x, y) = \mathcal{F}_{\xi\eta}^{-1}[\tilde{\mathbf{k}}_U(\xi, \eta)\tilde{H}(\omega, \xi, \eta)](x, y), \quad (39)$$

$$\tilde{\mathbf{k}}_U(\xi, \eta) = \tilde{a}_U(\xi, \eta)\tilde{\mathbf{g}}(\xi, \eta), \quad (40)$$

$$\tilde{a}_U(\xi, \eta) = \frac{A}{Z}\tilde{c}(\xi, \eta) + 1 \quad (41)$$

for (16), (33), (35), and (36), respectively (where the subscript U means ‘uniform’ thickness). In this case, A corresponds to the thickness of the sheet. We can see that a thicker sheet induces a greater enhancing effect, provided that the plane sections of the sheet remain straight and perpendicular to the neutral surface (see Figure 10).

This speculation is supported by the result of a simple experiment similar to that described in section 2.2. Fourteen observers were given 6 seconds to rub across the surface of the experimental apparatus (illustrated in Figure 2) using two intermediate objects: a polyethylene (PE) sheet (thickness 0.06 mm) and a silicone rubber sheet ($25 \times 15 \times 3$ mm) whose bottom side was covered with a PE sheet (thickness 0.06 mm). Each observer performed 6 trials with each sheet. Thus, the total number of trials with each sheet was 84 (6 trials \times 14 observers). Numbers of trials with correct responses with the PE and silicone rubber sheets were 17 and 39, respectively. The difference was highly significant ($p = 2.64 \times 10^{-4}$, one-tailed Fisher’s exact test).

As we mentioned in the beginning of this paper, the sheet metal inspectors in automobile factories know that knit work gloves contribute to the detection of surface undulation. The structure of the fabric of the knit work glove initially suggested the basic structure of the tactile contact lens. Figures 11(a) and (b) show the enhanced views of the work glove fabric. The sheet metal inspectors usually move their hands in the finger-to-wrist direction, which is the x direction in Figures 11(a) and (b). This structure results in discrete distribution of the contact areas on the skin surface. Moreover, it may also have the lever mechanism illustrated in Figure 11(c). Although this speculation needs to be verified experimentally, several technical problems have prevented us from developing effective stimuli. This will be a topic of future work.

4.2 Tactile sensing mechanisms

Fearing and Hollerbach [1985] predicted that the epidermal ridges play a role in enhancing the amplitude of the strain. This is because the incompressible material (in this case, the skin) is a band-pass filter from the surface force to the strain. This effect of the epidermal ridges is the same as that represented by the second term of (35), i.e., the spatial aliasing effect resulting from the discrete contact. Borrowing Fearing and Hollerbach’s term, this mechanism is similar to the electrical chopper that converts a DC voltage into an AC voltage.

The lever effect also seems to exist in the natural human skin. As shown in

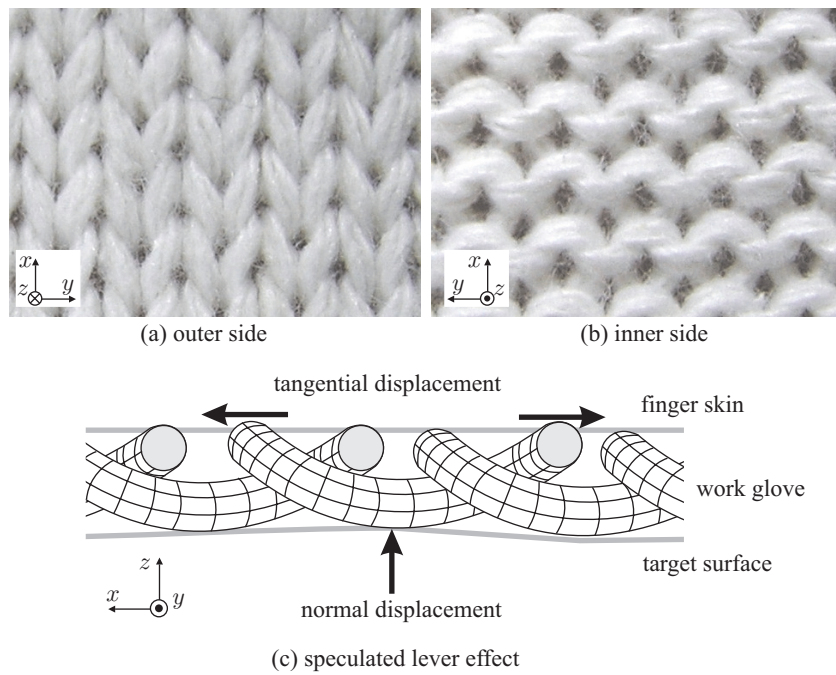


Fig. 11. The structure and mechanics of the work glove fabric (x direction in the figures corresponds to the finger-to-wrist direction).

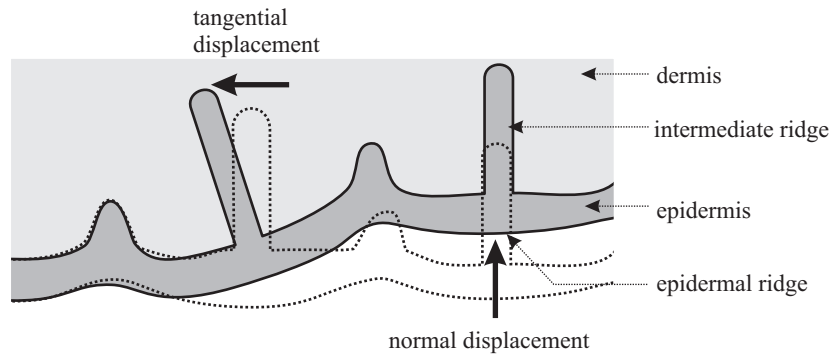


Fig. 12. Speculated lever effect in the human glabrous skin.

Figure 12, the epidermis has ridges projecting into the dermis. It has long been speculated [Cauna 1954] that the intermediate ridges, which are located below the epidermal ridges, act as magnifying levers for the transmission of tactile stimuli, although this has not been experimentally verified. This effect may be similar to the lever effect described by the first term of (35).

From a biomimetic perspective, these points will also be worth considering in designing tactile sensors that could be used as artificial skin for robots.

4.3 Tactile/haptic display devices

Some of the tactile display devices under development use actuated pin arrays for displaying normal displacement (or force) on the skin surface [Moy et al. 2000; Lee et al. 2003; Wagner et al. 2004]. In contrast, tactile display devices that generate distributed lateral (tangential) displacement (or force) have recently been proposed [Hayward and Cruz-Hernández 2000; Pasquero and Hayward 2003; Pasquero et al. 2004]. Relation (27) implies that this type of tactile display devices may be capable of generating a sensation equivalent to that generated by the normal displacement-type tactile display devices.

Substitution of normal displacement by tangential force or displacement has been used to display undulating surfaces through a two-dimensional, joy-stick type haptic display device [Minsky et al. 1990]. It is experimentally demonstrated that the contribution of the tangential force is larger than that of the actual trajectory of the fingertip in perceiving surface geometry through scanning touch [Robles-De-La-Torre and Hayward 2001]. In these cases, the force is applied to the overall surface of the hand or finger. Relation (27) implies that a similar effect can be obtained by controlling the tangential displacement distribution on the finger skin.

4.4 Future work on the modeling method

Future research should include quantitative evaluation of the validity of the simple model described in section 3. For this purpose, the model should be compared with more accurate (and computationally expensive) models, which would include the bone beneath the skin, the layers of the skin, the epidermal ridges, etc.

Design optimization of the tactile contact lens is also an important topic for study. The model described in section 3 has limitations to be used for the optimization, but can be a first step toward this goal. This model may be used to predict the strain pattern in the skin tissue produced by a given geometric distribution of contact area. Further studies, however, are needed to consider the bending of the pins and the deflection of the base sheet. Moreover, in order to relate the strain pattern to the perceived magnitude of undulation, we may need some additional knowledge or assumptions concerning the mechanoreceptors' temporal frequency response to every element of the strain tensor.

It will also be important to compare the importance of the reduction of friction with the effect of the pins. Influence of the tangential force resulting from the friction may be evaluated if the mechanoreceptors' temporal frequency response to every element of the strain tensor is known. It is, however, not straightforward to consider the vibrations induced by the friction. In order to identify the influence of the vibrations, dynamic characteristics of the skin, the target surface, and the intermediate material will need to be considered. Adequate models of the microscopic structures of the surfaces may also be required.

5. CONCLUDING REMARKS

In this paper, we have introduced the “tactile contact lens,” which is a sheet-like device for enhancing haptic detection of surface undulation through scanning touch. The effectiveness of this device is supported by the results of a psychophysical experiment. We have presented a mathematical analysis suggesting two explanations

for the enhancing effect. One is the lever-like behavior of the pins that generates tangential displacement on the skin surface. The second is the combination of the spatial aliasing effect induced by the discrete contact and the band-pass filtering characteristic of the incompressible elastic material (i.e., the finger skin). We have discussed the results of this analysis in relation to other sensitivity-enhancing materials, tactile sensing mechanisms, and tactile/haptic display devices. Future improvements and potential applications of the analysis method have also been discussed.

APPENDIX

In this appendix section, we describe the derivations of the Fourier transforms of $\mathbf{K}_{uf}(x, y)$ and $\mathbf{K}_{\varepsilon f}(x, y)$, which appear in section 3.4. Now let the following function be defined:

$$f(x, y, z) = \frac{1}{\sqrt{x^2 + y^2 + z^2}}.$$

The Fourier transform of $f(x, y, z)$ over x and y is given by

$$\begin{aligned} \tilde{f}(\xi, \eta, z) &= \int_{-\infty}^{\infty} \int_{-\infty}^{\infty} \frac{1}{\sqrt{x^2 + y^2 + z^2}} e^{-j(x\xi + y\eta)} dx dy \\ &= \int_0^{2\pi} \int_0^{\infty} \frac{1}{\sqrt{r^2 + z^2}} e^{-jr\rho(\cos\theta \cos\phi + \sin\theta \sin\phi)} r dr d\theta \\ &= \int_0^{\infty} \int_0^{2\pi} \frac{r}{\sqrt{r^2 + z^2}} e^{-jr\rho \cos(\theta - \phi)} d\theta dr \\ &= \int_0^{\infty} \frac{2\pi r}{\sqrt{r^2 + z^2}} J_0(r\rho) dr \\ &= \frac{2\pi e^{-z\sqrt{\xi^2 + \eta^2}}}{\sqrt{\xi^2 + \eta^2}}, \end{aligned}$$

where $\rho = \sqrt{\xi^2 + \eta^2}$, and $J_0(\cdot)$ is the zero-order Bessel function of the first kind. Here we used the following properties of the Bessel function [Bowman 1958]:

$$\int_0^{2\pi} e^{ja \cos\theta} d\theta = 2\pi J_0(a) \quad \text{and} \quad \int_0^{\infty} \frac{x J_0(bx)}{\sqrt{a^2 + x^2}} dx = \frac{e^{-ab}}{b}.$$

All elements of $\mathbf{K}_{uf}(x, y)$ and $\mathbf{K}_{\varepsilon f}(x, y)$ can be written by using $f(x, y, z)$. For example, the (1, 1)-th elements of $\mathbf{K}_{uf}(x, y)$ and $\mathbf{K}_{\varepsilon f}(x, y)$ are respectively written as follows:

$$\begin{aligned} \frac{3}{4\pi E} \frac{2x^2 + y^2}{(x^2 + y^2)^{3/2}} &= -\frac{3}{4\pi E} \left(2x \frac{\partial f(x, y, 0)}{\partial x} + y \frac{\partial f(x, y, 0)}{\partial y} \right), \\ \frac{3}{4\pi E} \frac{x(-2x^2 + y^2 + Z^2)}{(x^2 + y^2 + Z^2)^{2/5}} &= -\frac{3}{4\pi E} \cdot x \cdot \frac{\partial^2 f(x, y, Z)}{\partial x^2}. \end{aligned}$$

The Fourier transform has the following properties:

$$\mathcal{F}_x \left[\frac{\partial \phi(x)}{\partial x} \right] (\xi) = j\xi \cdot \tilde{\phi}(\xi) \quad , \quad \mathcal{F}_x [x \cdot \phi(x)] (\xi) = j \frac{\partial \tilde{\phi}(\xi)}{\partial \xi},$$

where $\phi(x)$ is an arbitrary function of x , and $\tilde{\phi}(\xi) = \mathcal{F}_x[\phi(x)](\xi)$. By using these properties, the Fourier transform of $\mathbf{K}_{uf}(x, y)$'s (1,1)-th element is given as follows:

$$\begin{aligned} \mathcal{F}_{xy} \left[\frac{3}{4\pi E} \frac{2x^2 + y^2}{(x^2 + y^2)^{3/2}} \right] (\xi, \eta) &= -\frac{3}{4\pi E} \mathcal{F}_{xy} \left[2x \frac{\partial f(x, y, 0)}{\partial x} + y \frac{\partial f(x, y, 0)}{\partial y} \right] (\xi, \eta) \\ &= \frac{3}{4\pi E} \left(2 \frac{\partial}{\partial \xi} (\xi \cdot \tilde{f}(\xi, \eta, 0)) + \frac{\partial}{\partial \eta} (\eta \cdot \tilde{f}(\xi, \eta, 0)) \right) \\ &= \frac{3}{2E} \frac{\xi^2 + 2\eta^2}{(\xi^2 + \eta^2)^{3/2}}. \end{aligned}$$

The Fourier transform of $\mathbf{K}_{ef}(x, y)$'s (1,1)-th element is given as follows:

$$\begin{aligned} \mathcal{F}_{xy} \left[\frac{3}{4\pi E} \frac{x(-2x^2 + y^2 + Z^2)}{(x^2 + y^2 + Z^2)^{2/5}} \right] (\xi, \eta) &= -\frac{3}{4\pi E} \mathcal{F}_{xy} \left[x \cdot \frac{\partial^2 f(x, y, Z)}{\partial x^2} \right] (\xi, \eta) \\ &= -\frac{3j}{4\pi E} \frac{\partial}{\partial \xi} (-\xi^2 \cdot \tilde{f}(\xi, \eta, Z)) \\ &= \frac{3je^{-Z\rho} \xi (\xi^2(1 - Z\rho) + 2\eta^2)}{2\pi E \rho^3}. \end{aligned}$$

All other elements of $\tilde{\mathbf{K}}_{uf}(\xi, \eta)$ and $\tilde{\mathbf{K}}_{ef}(\xi, \eta)$ can be obtained in the same manner.

ACKNOWLEDGMENTS

This work has been supported by Toyota Motor Corporation. We thank the engineers and craftsmen in Motomachi Plant of Toyota Motor Corporation who motivated and inspired our research.

REFERENCES

- BOWMAN, F. 1958. *Introduction to Bessel Function*. Dover.
- CAUNA, N. 1954. Nature and functions of the papillary ridges of the digital skin. *Anatomical Record* 119, 449–468.
- DANDEKAR, K., RAJU, B. I. AND SRINIVASAN, M. A. 2003. 3-D finite-element models of human and monkey fingertips to investigate the mechanics of tactile sense. *Journal of Biomechanical Engineering* 125, 682–691.
- FEARING, R. S. 1990. Tactile sensing mechanisms. *International Journal of Robotics Research* 9, 3, 3–23.
- FEARING, R. S. AND HOLLERBACH, J. M. 1985. Basic solid mechanics for tactile sensing. *International Journal of Robotics Research* 4, 3, 40–54.
- GORDON, I. E. AND COOPER, C. 1975. Improving one's touch. *Nature* 256, 203–204.
- HAYWARD, V. AND CRUZ-HERNÁNDEZ, J. M. 2000. Tactile display device using distributed lateral skin stretch. In *Proceedings of 8th Symposium on Haptic Interfaces for Virtual Environment and Teleoperator Systems*. 1309–1314.
- LAMOTTE, R. H. AND SRINIVASAN, M. A. 1987. Tactile discrimination of shape: responses of slowly adapting mechanoreceptor afferents to a step stroked across the monkey fingerpad. *Journal of Neuroscience* 7, 1655–1671.
- LEDERMAN, S. J. 1978. “Improving one's touch” ... and more. *Perception and Psychophysics* 24, 2, 154–160.
- LEE, J. M., WAGNER, C. R., LEDERMAN, S. J., AND HOWE, R. D. 2003. Spatial low pass filter for pin actuated tactile displays. In *Proceedings of the 11th Symposium on Haptic Interfaces for Virtual Environment and Teleoperator Systems*. 57–62.
- LOVE, A. E. H. 1927. *A Treatise on the Mathematical Theory of Elasticity*, 4 ed. Dover.

- MAENO, T., KAZUMI, K., AND YAMAZAKI, N. 1998. Relationship between the structure of human finger tissue and the location of tactile receptors. *JSME International Journal* 41, 1, 94–100.
- MINSKY, M., OUH-YOUNG, M., STEELE, O., BROOKS, F. P. J., AND BEHENSKY, M. 1990. Feeling and seeing: Issues in force display. *Computer Graphics: A Quarterly Report of SIGGRAPH ACM* 24, 2, 235–243.
- MOY, G., SINGH, U., TAN, E., AND FEARING, R. S. 2000. Human psychophysics for teletaction system design. *Haptics-e, The Electronic Journal of Haptics Research (www.haptics-e.org)* 1, 3.
- NELSON, B. J. AND MITAL, A. 1995. An ergonomic evaluation of dexterity and tactility with increase in examination/surgical glove thickness. *Ergonomics* 38, 4, 723–33.
- PASQUERO, J. AND HAYWARD, V. 2003. STReSS: A practical tactile display system with one millimeter spatial resolution and 700 Hz refresh rate. In *Proceedings of The 3rd European Conference on Haptics*. 94–110.
- PASQUERO, J., LÉVESQUE, V., HAYWARD, V., AND LEGAULT, M. 2004. Display of virtual braille dots by lateral skin deformation: A pilot study. In *Proceedings of The 4th European Conference on Haptics*. 96–103.
- PERRY, D. A. AND WRIGHT, H. E. 1987. Touch enhancing pad. *US Patent #4657021*.
- PHILLIPS, J. R. AND JOHNSON, K. O. 1981. Tactile spatial resolution III. a continuum mechanics model of skin predicting mechanoreceptor responses to bars, edges, and gratings. *Journal of Neurophysiology* 46, 6, 1204–1225.
- ROBLES-DE-LA-TORRE, G. AND HAYWARD, V. 2001. Force can overcome object geometry in the perception of shape through active touch. *Nature* 412, 445–448.
- SHIBATA, M. AND HOWE, R. D. 1999. Effect of gloving on perceptual and manipulation task performance. In *Proceedings of the ASME Dynamic Systems and Control Division*. DSC-Vol. 67. 6–18.
- WAGNER, C. R., LEDERMAN, S. J., AND HOWE, R. D. 2004. Design and performance of a tactile shape display using RC servomotors. *Haptics-e, The Electronic Journal of Haptics Research (www.haptics-e.org)* 3, 4.

Received xx xxx; revised xx xxx; accepted xx xxx;